UC Santa Barbara

Title

Familial Alzheimer's Disease Mutations Differentially Alter Amyloid β-Protein Oligomerization

Permalink

https://escholarship.org/uc/item/4v17s2b9

Journal

ACS Chemical Neuroscience, 3(11)

ISSN

1948-7193

Authors

Gessel, Megan Murray
Bernstein, Summer
Kemper, Martin
et al.

Publication Date

2012-11-21

**DOI**

10.1021/cn300050d

Peer reviewed

Familial Alzheimer's Disease Mutations Differentially Alter Amyloid β-Protein Oligomerization

Megan Murray Gessel,*,[†] Summer Bernstein,[†] Martin Kemper,[†] David B. Teplow,[‡] and Michael T. Bowers[†]

[†]Department of Chemistry and Biochemistry, University of California, Santa Barbara, California 93106, United States

[‡]Department of Neurology, David Geffen School of Medicine at UCLA, Mary S. Easton Center for Alzheimer's Disease Research at UCLA, and Brain Research Institute and Molecular Biology Institute, University of California at Los Angeles, Los Angeles, California 90095, United States

Ⓢ Supporting Information

ABSTRACT: Although most cases of Alzheimer's disease (AD) are sporadic, ∼5% of cases are genetic in origin. These cases, known as familial Alzheimer's disease (FAD), are caused by mutations that alter the rate of production or the primary structure of the amyloid β-protein (Aβ). Changes in the primary structure of Aβ alter the peptide's assembly and toxic activity. Recently, a primary working hypothesis for AD has evolved where causation has been attributed to early, soluble peptide oligomer states. Here we posit that both experimental and pathological differences between FAD-related mutants and wild-type Aβ could be reflected in the early oligomer distributions of these peptides. We use ion mobility-based mass spectrometry to probe the structure and early aggregation states of three mutant forms of Aβ40 and Aβ42: Tottori (D7N), Flemish (A21G), and Arctic (E22G). Our results indicate that the FAD-related amino acid substitutions have no noticeable effect on Aβ monomer cross section, indicating there are no major structural changes in the monomers. However, we observe significant changes to the aggregation states populated by the various Aβ mutants, indicating that structural changes present in the monomers are reflected in the oligomers. Moreover, the early oligomer distributions differ for each mutant, suggesting a possible structural basis for the varied pathogenesis of different forms of FAD.

KEYWORDS: Alzheimer's disease, amyloid β-protein, ion mobility mass spectrometry
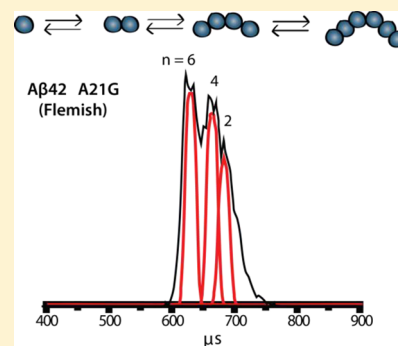
Amyloid β-protein (Aβ) self-assembly has been shown to play an important role in Alzheimer's disease (AD).[1] *In vivo*, Aβ exists primarily as a 40- or 42-residue protein (Aβ40 and Aβ42). Although Aβ40 is much more abundant, Aβ42 is significantly more toxic.[2] Aβ42 and Aβ40 also aggregate via distinct pathways; Aβ40 forms small oligomers (dimers and tetramers), while Aβ42 forms these and larger assemblies (e.g., hexamers through dodecamers).[3] One compelling piece of evidence connecting Aβ with AD is its role in genetic forms of the disease, known as familial AD (FAD).

Most cases of AD are sporadic; however approximately 5% of cases are genetic.[4] FAD is attributed to mutations in either the presenilin 1 gene on chromosome 14,[5] the presenilin 2 gene on chromosome 14,[6] or the amyloid precursor protein (APP) gene on chromosome 21.[7] Most FAD cases are the result of mutations to the presenilins that increase the ratio of Aβ42 to Aβ40 by altering the enzymatic cleavage of γ-secretase.[8] FAD-related mutations in the APP sequence may occur either outside or inside the Aβ region. For this work, we are interested in the latter type, specifically the Tottori (D7N),[9] Flemish (A21G),[10] and Arctic (E22G)[11] mutations of Aβ40 and Aβ42, due to the differences in their pathological and biochemical properties.

The Tottori mutation, D7N, is found in a Japanese family whose affected members develop AD at 60−65 years of age.[9] Carriers of the Tottori mutation exhibit typical AD pathology (plaques and tangles) and no cerebrovascular events.[9] *In vitro* studies have shown that this mutation promotes the elongation phase of fibril formation, although protofibril levels were shown to be lower compared with wild-type (wt) Aβ.[12] In another study, the Tottori form of both Aβ40 and Aβ42 exhibited an accelerated secondary structure transition from random coil to β-structure and an increased propensity to form larger assemblies. The oligomers described in these experiments were more structured than those of wt Aβ and much more toxic to cells. Interestingly, the relative increase in aggregation propensity and toxicity was larger for Aβ40 than for Aβ42,[13] although this may be due to the overall lower toxicity of wt Aβ40.

Carriers of the Flemish mutation, A21G, develop AD in their 40s and have significant amyloid accumulation in brain blood

vessel walls (cerebral amyloid angiopathy; CAA) as well as parenchymal amyloid plaques. Thus, the clinical presentation is one involving both hemorrhagic stroke and progressive dementia.[10,14] Two causes of early onset AD with the Flemish mutant have been suggested. First, the A21G substitution, which is in close proximity to the α-secretase cleavage site in APP, has been shown to promote production of Aβ by decreasing the amount of α-secretase cleavage within the Aβ sequence.[15] This change is not observed in the cases of nearby FAD-related substitutions at E22 and D23. Others have suggested that the peptide's unique aggregation properties are responsible for its disease phenotype. The Flemish substitution leads to decreased β-sheet formation[16] and decreased fibril extension[18] compared with wild-type. Despite these negative effects on fibril formation, the A21G substitution enhances formation of protofibrils. Another study demonstrated that the Flemish mutant forms fewer large oligomers compared with wt Aβ.[17] This result suggests that the mutation allows the protein to stay in more toxic intermediate assemblies, rather than going on to form less toxic amyloid fibrils.

The Arctic mutation, E22G, originates from a family in northern Sweden and results in a disease onset at ~57 years.[11] Like the Tottori mutant, this mutation does not lead to the same cerebrovascular problems that many FAD-related mutations cause.[10,18] However, unlike the Tottori mutant, the E22G substitution *increases* the rate of protofibril formation compared with wt Aβ.[11] Another study demonstrated that Aβ40 E22G forms larger aggregates than wt Aβ40, although Aβ42 E22G formed similar sized aggregates to wt Aβ42.[17] An *in vivo* study demonstrated that soluble Aβ E22G could inhibit long-term potentiation, suggesting that a nonfibrillar, soluble form of this peptide was primarily responsible for Aβ-related cognitive deficits.[19] A second *in vivo* study had similar results, linking the presence of a 56 kDa dodecameric species (termed "Aβ*56"), with the onset of AD-related cognitive problems.[20]

Studies suggest that the early oligomer states of Aβ constitute the most toxic forms of the peptide and may be the primary species responsible for Aβ-related cell damage.[1,20,21] Because of this, we wondered whether reported differences in the pathological and biochemical properties of various FAD-related Aβ mutants might be reflected in the early oligomer distribution of these peptides. Ion mobility mass spectrometry (IM-MS)[22] has already been successfully used to elucidate the early oligomerization of wt Aβ.[3a,b] In the work presented here, we use IM-MS to probe the structure and early aggregation states of the Tottori, Flemish, and Arctic FAD mutants of Aβ40 and Aβ42. Our results indicate that the FAD-related substitutions have no measurable effect on Aβ monomer cross sections (see Table 1), indicating there are no major structural changes in the monomers. However, we observe significant changes to the aggregation states populated by the

various FAD Aβ mutants, suggesting that structural changes in the monomers are reflected in the peptide assemblies. Moreover, the early oligomer distributions differ for each mutant, suggesting a structural basis for the varied pathogenesis of different forms of FAD.

■ RESULTS

Mass Spectrometry. All Aβ40 or Aβ42 mutants have mass spectra showing at least the $z/n = -4$, -3, and $-5/2$, peaks, where z is the charge and n is the oligomer size. The mass spectrum for the Aβ40 Tottori mutant (D7N) is shown as an example in Figure 1 (see Figure S1, Supporting Information, for all other mass spectra). In some spectra, $z/n = -5$ and -2 were also observed.
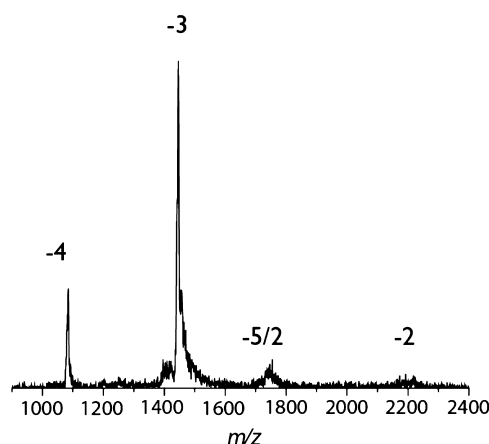

Figure 1. Mass spectrum of Aβ40 D7N, the Tottori mutant. Peaks corresponding to $z/n = -4$, -3, -2, and $-5/2$ are present, where z is the charge and n is the oligomer size. Mass spectra of all other alloforms considered here are given in Supporting Information, Figure S1.

Ion Mobility and the Monomer Structure. Ion mobility experiments were first performed in order to examine the effects of FAD-related substitutions on the monomer structure of Aβ40 and Aβ42. Figure 2 shows the ATD of $z/n = -3$ for wt Aβ40 and Aβ40 D7N, as examples. Both ATDs consists of two partially resolved features at ~625 and ~660 μs. Previous analysis of $z/n = -3$ wt Aβ identified the feature at ~625 μs as a compact, gas-phase structure and the feature at ~660 μs as an extended, solution-like structure.[23] Although MD simulations have not been completed for the mutant peptides, we expect this to be the case here, as well. Increasing the injection voltage provides further confirmation that these peaks are monomer species (see Figure S3, Supporting Information). In the ATD of Aβ40 D7N, an additional peak at ~500 μs is present as well. At high injection voltages this peak is diminished, indicating it most likely corresponds to a larger assembly that dissociates into monomer Aβ (Figure S3, Supporting Information). The Tottori mutant is the only mutant that contains this additional feature at early arrival time in the ATD of $z/n = -3$.

The $z/n = -3$ ATDs for the other alloforms may be found in the Supporting Information, and all consist of two overlapping peaks (Figure S2, Supporting Information). Experimental cross sections were measured for each dehydrated monomer alloform, and the mutant versions show cross sections similar to wt Aβ (Table 1). For example, wt Aβ40 has a cross section of 679 Å^2 and the Aβ40 D7N mutant has a cross section of 670

Table 1. Experimental Cross Sections and Standard Deviations of Dehydrated Solution Monomer ($z = -3$) of Aβ40 and Aβ42 Peptides

	cross section (Å^2)	
	Aβ40	Aβ42
wt	679 ± 8	693 ± 8
D7N	670 ± 6	701 ± 10
A21G	670 ± 9	712 ± 8
E22G	664 ± 7	699 ± 7

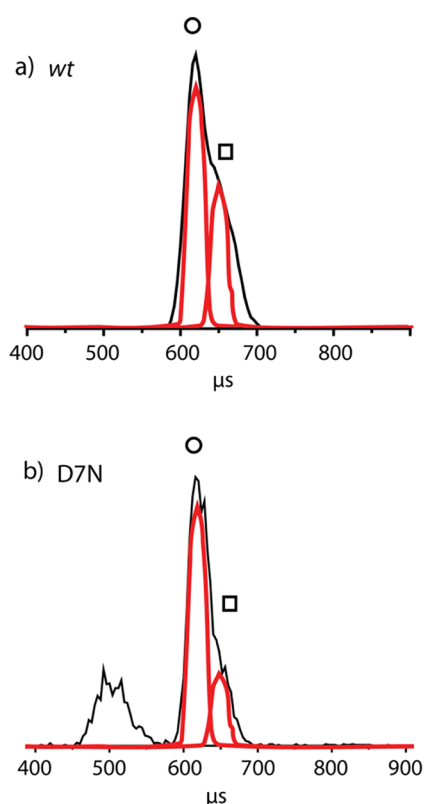**Figure 2.** Plots of the $z/n = -3$ ATD of (a) wt Aβ40 and (b) Aβ40 D7N. Two overlapping peaks represent a gas phase structure (O) and dehydrated solution structure ($\square$). See ref 28 for a detailed discussion of this assignment. A peak at $\sim$500 μs in the Aβ40 D7N ATD represents a larger assembly. The red peaks are theoretical representations of a single monomer isomer at the indicated arrival time (see eq 3).

Å^2. Although the IM-MS experimental collision cross section does not give a detailed picture of peptide structure, the results do suggest that large conformational changes in Aβ due to these single amino acid substitutions are unlikely. Although $z/n = -5$ and -4 peaks were often present in the mass spectra, they most likely arise during the electrospray process (Aβ is charged at -3 in solution), and hence their ATDs are not presented here. The -2 peak, when observed, was always too weak to yield a reliable ATD.

Ion Mobility and the Early Oligomer Distribution. Figure 3 shows ATDs of $z/n = -5/2$ for wt Aβ40 (panel a) and Aβ42 (panel b) at a low injection voltage (35 V). The ATD of wt Aβ40 contains two overlapping peaks, which we have previously assigned as dimer and tetramer Aβ40.[3a] Aβ42 shows additional features at shorter arrival times, which we have also previously assigned as dimer, tetramer, hexamer, decamer, and dodecamer Aβ42.[3a,b] Red lines indicate modeled, fitted arrival time distributions for each feature in the ATDs. The model uses transport equations to model arrival time distributions of ions with a given mobility (see Methods section). Notice that in each case, the experimental features are broader than the fitted line, indicating the presence of a family of oligomeric structures, not just a single structure. This is in contrast to the monomer peaks in Figure 2 where little structural variation is noted.

The Tottori Mutation, D7N. The $-5/2$ ATD of Aβ40 D7N has three features at $\sim$585, $\sim$645, and $\sim$675 μs (Figure 3c). At a high injection voltage of 100 V, the distribution is

shifted to the right, toward the feature at $\sim$675 μs (Figure 3e). No other features appear at longer arrival times, indicating that the feature at 675 μs is almost certainly a dimer. As described earlier, high injection voltages may cause large, noncovalent assemblies to disassemble into smaller subcomponents, so the features at $\sim$585 and 645 μs are most likely larger oligomers. Although high injection voltages may cause conformational rearrangements within protein structures and oligomer assemblies, it is unlikely that this is occurring here. Unraveling of a monomer within an oligomer at higher injection voltages, without dissociation, would lead to a broadening of the ATD and a shift to longer times (larger cross sections). What we observe is the larger oligomers decreasing in relative intensity but not broadening and the appearance of new sharp features that correlate in cross section with oligomers of smaller size. Therefore, we feel the dominant process occurring with increasing injection voltage is oligomer dissociation not structural change without dissociation.

The Aβ oligomers studied here are too large for analysis with current molecular dynamics methods. Instead, the cross sections of various oligomers (tetramer through dodecamer) were approximated with a simple structural model, which has been previously used to describe the oligomer states of wt Aβ.[3a] In this approximation, each dimer is formed by overlapping two spherical monomers (with radii determined by the monomer cross section) to yield a dimer cross section equal to that given by experiment. No further accommodation is made in building model structures for larger oligomers. Hence the model cross sections are upper limits of the expected experimental cross section for a given structure. Details of the modeling may be found in the Methods section and the Supporting Information.

The modeled structures for each mutant and corresponding cross sections are given in Table 2 (see Supporting Information for in-depth discussion of modeling). Based on the experimental cross sections, the features at $\sim$645 and $\sim$585 μs in the Aβ40 D7N $-5/2$ ATD can be assigned as a tetramer and hexamer, respectively. Comparison of experiment with the model indicates that the experimental tetramer cross section ($\sigma_{experiment} = 2177$ Å^2) best matches that of an extended, open arrangement (Table 2; $\sigma_{model} = 2204$ Å^2). As described in the Methods section, the model represents the largest possible cross section for a given arrangement (i.e., an upper limit). The similarity of the experimental cross sections and the cross sections of the modeled structures does not necessarily mean, for example, that the tetramer assumes this exact shape, but the experimental cross section is consistent with an extended, open shape. Note that the experimental ATD is broader than expected for a single structure indicating there is a family of tetramer structures for the D7N Aβ40 alloform. Similar analysis shows that the hexamer best corresponds to a planar, cyclical hexamer ($\sigma_{model} = 3067$ Å^2; $\sigma_{experiment} = 2741$ Å^2). Of interest is the fact that the tetramer of wt Aβ40 more closely resembles the planar square box than the open structure and did not add a dimer to form the planar hexamer.[3a] The open structures of the Tottori mutant tetramer allowed a hexamer to be formed by this Aβ40 alloform. Also note that the hexamer peak is much closer to the single structure calculation (red peak) indicating a much narrower structural family.

The ATD of $z/n = -5/2$ Aβ42 D7N is shown in Figure 3d. At a low voltage of 35 V, a dominant feature is present at $\sim$530 μs, with a trailing shoulder to longer times. Increasing the injection voltage shifts the distribution to later arrival times (Figure 3f). Two new peaks become apparent, one at 600 μs
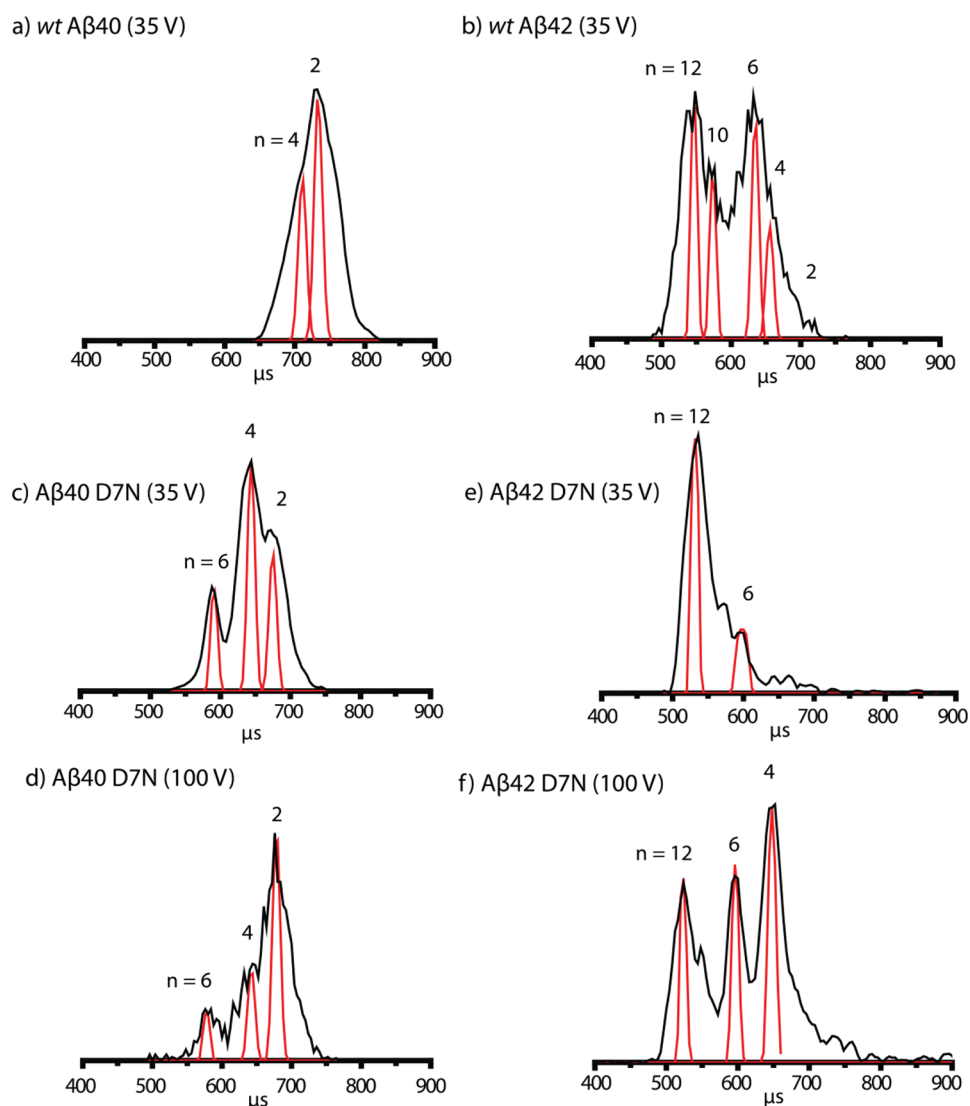
Figure 3. Arrival time distributions of $z/n = -5/2$ for (a) wt $A\beta40$ and (b) wt $A\beta42$ at an injection voltage of 35 V, where z is the charge and n is the oligomer size. ATDs of $z/n = -5/2$ are also given for (c,e) $A\beta40$ D7N and (d,f) $A\beta42$ D7N at injection voltages of 35 and 100 V, respectively. The narrow red peaks are calculated from eq 3 and are the width of a single isomer.

and the other stonger peak near 650 μs. Unresolved signal at longer arrival times is present, as well. The results of this injection voltage study suggest that both the 600 and 650 μs features result from dissociation of larger oligomers. The cross section of the feature at 650 μs indicates that this peak corresponds to a species larger than a dimer. If the species is a dimer, it has a cross section of 1090 Å^2, a cross section that is ~10% smaller than any dimer formed by other $A\beta42$ alloforms. Therefore, a more reasonable assignment for this feature is that of a tetramer with a cross section of 2180 Å^2, a value in line with other tetramer cross sections. Although no dimer peak is apparent in the ATD, it is very possible that trailing signal between ~700 and ~800 μs could contain some dimer, although no peaks are resolved.

Comparison with the modeled cross sections shown in Table 2 indicates that the feature at ~600 μs most closely corresponds to a planar, hexamer ring (σ_{model} = 2944 Å^2; $\sigma_{experiment}$ = 2676 Å^2) and the one at 650 μs to an open tetramer (σ_{model} = 2188 Å^2; $\sigma_{experiment}$ = 2180 Å^2). Since these features are only weakly present at low injection energies, they are probably not abundant in solution. The feature at the shortest arrival time

corresponds well with a dihexamer (σ_{model} = 4605 Å^2; $\sigma_{experiment}$ = 4260 Å^2). Note that even at a high injection energy this large assembly is still present, indicating that the dodecamer of D7N is particularly stable and resistant to dissociation. The dodecamer assembly of wt $A\beta42$ is also stable at high injection energies[3a,b] but is not as abundant as the Tottori D7N mutant, shown here.

The Flemish Mutation, A21G. The ATD of the $z/n = -5/2$ of the Flemish mutant (A21G) of $A\beta40$ contains two strongly overlapping features at ~675 and ~700 μs (Figure 4a). Increasing the injection energy shifts the distribution toward higher arrival times and suggests that the feature at ~700 μs is a dimer. The measured experimental cross section of the feature at ~675 μs (σ_{model} = 2176 Å^2; $\sigma_{experiment}$ = 2172 Å^2) most closely matches the model for an extended (open) tetramer (See Table 2 for cross sections of all modeled tetramers).

Figure 4b shows the ATD for the $z/n = -5/2$ of the $A\beta42$ A21G. At low injection voltage, three overlapping features are present at ~615, ~670, and 690 μs. At high injection voltage (see Supporting Information), the distribution shifts to longer arrival times, suggesting that the peaks at 615 and 670 are

Table 2. Modeled Structures and Corresponding Cross Sections for Each Mutant[a]

		Cross section (Å²)*										
		D7N Aβ40		D7N Aβ42		A21G Aβ40		A21G Aβ42		E22G Aβ40		E22G Aβ42
n	Structure	Model	Exp	Model	Exp	Model	Exp	Model	Exp	Model	Exp	Model Exp
2		1200	1200	n/a†		1173	1173	1208	1208	1236	1236	n/a†
4		2204	2177	2188	2180	2192	2172	2284	2240	2215	2224	
		2140		2127		2170		2251		2150		n/a
		1981		1994		1910		1981		1968		
		1686		1767		1688		1793		1624		
6		3217		3321				3235	2976	3257		3315
		3067	2741	2944	2676	n/a		3042		2923	2688	2932 2664
		2443		2512				2419		2309		2508
12		n/a		5513		n/a		n/a		5488		5504
				4605	4260					4502	4320	4596 4380

[a]Experimental cross sections of features in the ATDs are included as well, next to the matching modeled cross section. In some cases, experimental cross sections were not obtained due to the absence of certain species in the ATDs. These are noted in the table (n/a). The asterisk indicates that as described in the Methods section, modeled cross sections represent the largest possible value for a given structure. The dagger indicates that Aβ42 E22G and D7N mutants did not show any resolved dimers peaks in the $z/n = -5/2$ ATDs. Because of this, the effective overlap of wt Aβ42 was used in both cases and no modeled and experimental dimer values are given in Table S1, Supporting Information, for these alloforms.
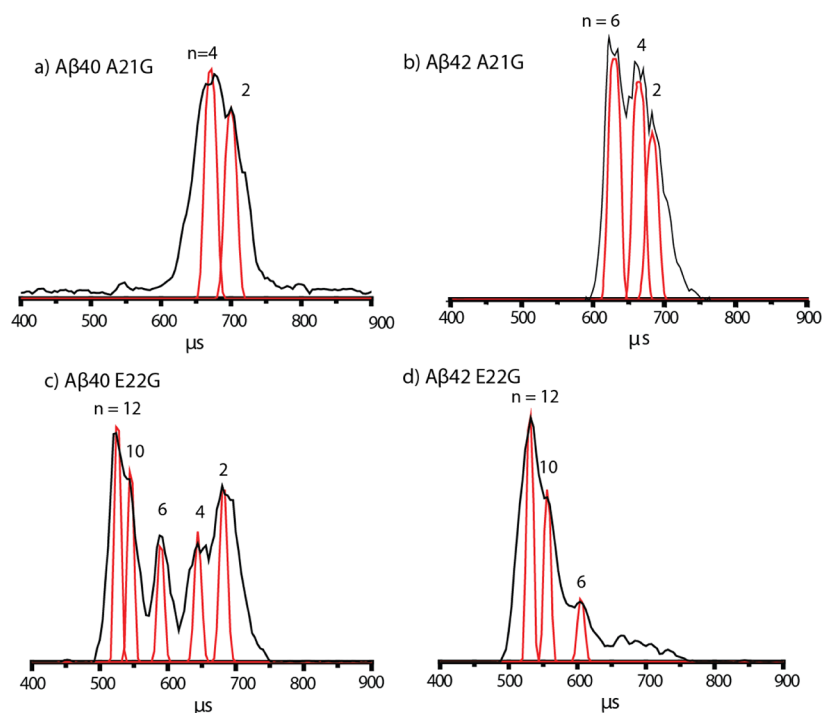
Figure 4. Arrival time distributions of $z/n = -5/2$ for the Flemish mutant (A21G) of (a) Aβ40 and (b) Aβ42 and the Arctic mutant (E22G) of (c) Aβ40 and (d) Aβ42, where z is the charge and n is the oligomer size. All ATDs were recorded with an injection voltage of 35 V. The narrow red peaks are calculated from eq 3 and are the width of a single isomer.

species larger than a dimer. No new peaks appear at arrival times longer than 690 μs, indicating that this feature corresponds to dimer Aβ42 A21G (Figure S4, Supporting Information). The modeling of these features provides additional information on their structures. For Aβ40, an open, near linear tetramer is most consistent with the experimental cross section. Based on experience with other systems, we would expect that this open tetramer would form a hexamer, but we do not observe one under our experimental conditions.

For Aβ42 of the Flemish mutant, an open tetramer is also observed, and in this case a hexamer is also formed (Table 2).

However, the experimental cross section of the hexamer is only 2% smaller than predicted for a cyclic planar hexamer. In all other systems where a planar cyclic hexamer is observed, the experimental cross section is about 10% smaller than the model cross section, as expected from structural accommodation (see the Supporting Information for a more detailed discussion of this effect). However, the hexamer cross section for the Flemish mutant is about 9% smaller than the open chain hexamer, strongly suggesting an open structure for this species. All other $A\beta 42$ alloforms form dodecamers that are unambiguously composed of two stacked hexamer rings. The fact that A21G does not form a dodecamer suggests that its hexamer structure is not a hexamer ring, a suggestion consistent with the assignment of the A21G hexamer to an open quasi-linear structure.

The Arctic Mutation, E22G. The $z/n = -5/2$ ATD of the $A\beta 40$ Arctic mutant (E22G) is given in Figure 4c. Several features are present, including peaks at ~515, ~540, ~590, ~640, and ~675 μs. An injection energy study (Figure S5) and comparison to modeled structures (Table 2) suggest that the peaks at ~675 and ~640 μs can be assigned as a dimer and an extended, open tetramer (σ_{model} = 2215 Å^2; $\sigma_{experiment}$ = 2224 Å^2), respectively. While it is surprising that the experimental cross section of the tetramer is slightly larger than the modeled cross section (the modeled cross sections represent the largest possible values, as described in the Methods section), these values are within the experimental error (1−2%).

The features at ~590, ~540, and ~515 μs indicate the presence of a planar hexamer ring (σ_{model} = 2923 Å^2; $\sigma_{experiment}$ = 2688 Å^2), a stacked decamer (σ_{model} = 4032 Å^2; $\sigma_{experiment}$ = 3880 Å^2), and a stacked dodecamer (σ_{model} = 4502 Å^2; $\sigma_{experiment}$ = 4320 Å^2), respectively. Interestingly, increasing the injection energy to 100 V does not appear to diminish the peaks that correspond to a dodecamer and decamer of $A\beta$, suggesting that these structures are especially stable, consistent with the fact that E22G is the only $A\beta$ alloform that forms a dodecamer. The features that correspond to hexamer, tetramer, and dimer species, however, are greatly diminished at this high injection voltage (Figure S5, Supporting Information).

The ATD of $z/n = -5/2$ $A\beta 42$ E22G contains features at ~525, ~575, and ~600 μs (Figure 4d). The high mobilities of the species at ~525 and ~575 μs suggest that these correspond to large oligomers of $A\beta$. Increasing the injection voltage shows a small increase in the intensity of the peak at ~600 μs and an increase in the broad signal between 650 and 750 μs; however the two overlapping features at short arrival times still dominate, similar to the case of $A\beta 40$ E22G. Comparison with the model cross sections in Table 2 indicates that the cross sections of the features at ~525 and ~560 μs best correspond to decamer and dodecamer of $A\beta 42$ E22G (decamer σ_{model} = 3770 Å^2, σ_{E22G} = 3740 Å^2; dodecamer σ_{model} = 4596 Å^2; $\sigma_{experiment}$ = 4380 Å^2). The feature at ~655 μs corresponds to a planar, ring-shaped hexamer (σ_{model} = 2932 Å^2; $\sigma_{experiment}$ = 2664 Å^2).

■ DISCUSSION AND CONCLUSIONS

FAD-related mutations produce amino acid substitutions in $A\beta$ that alter both the physical biochemistry of the peptide and its contributions to AD pathogenesis.[9−19,24] Because oligomers appear to play an important, and perhaps dominant, role in $A\beta$ toxicity, it seems reasonable that these oligomer distributions and structures could well relate to the mechanisms of the pathology of these systems. We chose to focus on the Tottori

(D7N), Flemish (A21G), and Arctic (E22G) mutations in this paper due to the varied properties that have been reported in the literature for each alloform.

Interestingly, in all three cases, the cross section of monomer $A\beta$ did not change significantly with mutation (Table 1). Although the cross section does not give detailed, atomic-level structural information about a protein, this result does suggest that there are no large conformational changes in monomer structure (i.e., it is unlikely that there is a transition to an extended β-structure at the monomer stage). These mutations do, however, lead to large differences in the oligomer distributions of the peptides, compared with their wt analogs.

Wild-type $A\beta 40$ only forms monomer through tetramer in our experiments (Figure 3a; Scheme 1a).[3a] However, the

Scheme 1. Mechanisms of Early Oligomer Formation of (a) $A\beta 40$ wt, (b) $A\beta 40$ A21G, (c) $A\beta 40$ D7N, and (d) $A\beta 40$ E22G[a]
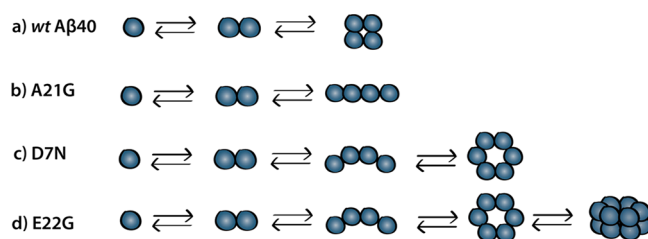

[a]Normally, wt $A\beta 40$ forms monomer, dimer, and tetramer, where the structure of the tetramer is closed. The D7N and E22G mutations allow the peptide to form larger oligomers like a hexamer and even, in the case of E22G, a dodecamer. Of interest is the fact that the A21G mutant forms an open tetramer but no hexamer suggesting a different kind of interfacial bonding for this alloform.

Tottori mutant can form a hexamer as well (Figure 3c; Scheme 1c). Interestingly, the hexamer formed by $A\beta 40$ D7N has a similar arrangement (compact, planar ring) to that of the hexamer formed by wt $A\beta 42$ (Figure 3b; Scheme 2a). However, unlike $A\beta 42$, no species larger than the hexamer appears in this experiment.

In the case of the $A\beta 42$ Tottori mutant, the dodecamer dominates at low injection voltage (Figure 3e). The cross section of this species suggests oligomeric structure similar that

Scheme 2. Mechanisms of Early Oligomer Formation of (a) $A\beta 42$ wt, (b) $A\beta 42$ D7N or $A\beta 42$ E22G, and (c) $A\beta 42$ A21G[a]
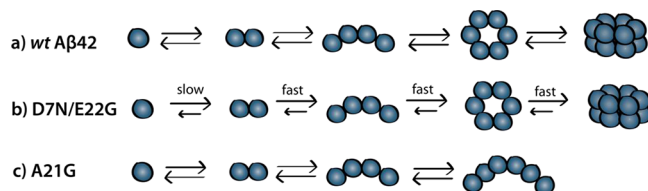
[a]D7N and E22G mutations are shown together due to the similarity of their mechanisms. Normally, wt $A\beta 42$ forms monomer through dodecamer. The D7N and E22G mutations increase the amount of dodecamer formed. The A21G mutation stops $A\beta 42$ oligomerization at the hexamer. Of more importance, the hexamer structue for this alloform is open, not a planar cylic ring like all other hexamers we observe in the other alloforms. Hence ring stacking is not available to it, and no dodecamer is formed along with decrease protofibril and fibril formation.

of to wt Aβ42: stacked hexamer rings. No other species were found at a low injection voltage in these experiments, besides monomer Aβ. Low injection voltages produce data that most represent the distribution of structures in solution, which suggest that this Aβ42 mutant exists predominantly as large oligomers in solution. Our past work with wt Aβ42 shows that wt Aβ42 forms decamer and dodecamer, but smaller assemblies (e.g., dimer and tetramer)[3a,b] are also abundant. The dominant formation of large oligomers for the D7N mutant is consistent with the increased rate of protofibril formation and fibril elongation reported for this peptide. The Aβ42 D7N hexamer and tetramer that dominate at high injection voltages are likely the products of the dissociation of larger assemblies and are likely not abundant in solution. Interestingly, the Aβ42 Tottori dodecamer and hexamer are still abundant at a high injection voltage, suggesting that these structures are very stable, even in the absence of solvent. The dodecamer assembly of wt Aβ42 is also stable at high injection voltages[3a,b] but not as stable as the Tottori D7N dodecamer reported here.

The formation of a stable dodecamer species for Aβ42 D7N but not by the Aβ40 mutant is curious. Previously, we suggested that a possible stacked hexamer arrangement of wt Aβ42 might be driven by association of the hydrophobic Aβ42 C-termini in the center of assembly.[3a,23] Without the additional residues I41 and A42, the tail of Aβ40 is less hydrophobic than Aβ42 and the association of Aβ40 D7N hexamers to form dodecamers may be less likely. The appearance of the cyclic hexamer structure for the Aβ40 isoform of D7N may be due to changes in intermolecular, electrostatic interactions between charged N-termini (interactions involving the seventh residue) or to a particularly stable hexamer conformation adopted by Aβ within these oligomers. The cross sections of Aβ40 and Aβ42 D7N oligomers are 5−10% smaller than those of wt, which indicates some structural differences between the two sets of oligomers. However, modeling indicates that the overall structures of Aβ D7N oligomers are similar to those of wt Aβ, suggesting that the D7N mutation primarily alters the stability of specific Aβ oligomers, not the overall aggregation pathway.

In many respects, the Arctic mutant (E22G) behaves similarly to the Tottori mutant. Both the Tottori and Arctic mutants have been reported to increase the range of the distribution of Aβ40 oligomers to larger sizes.[13,17] Here we report that both substitutions allow Aβ40 to access oligomeric states beyond those of wt Aβ40, consistent with these prior observations. One interesting difference between the two mutants, however, is that E22G Aβ40 forms decamer and dodecamer, which are not observed in the case of Aβ40 D7N (Figure 4c; Scheme 1c). The formation of a decamer and dodecamer species by Aβ40 E22G indicates that I41 and A42 are not absolutely necessary for the formation of these larger aggregates. Biochemical differences between the two peptides have been previously reported. Namely, the Tottori mutation decreases protofibril formation, while the Arctic mutation enhances protofibril formation.[12] The formation of dodecamer in the case of Aβ40 E22G but not Aβ40 D7N is consistent with this difference. In the case of Aβ42, neither mutant forms larger oligomers than wt Aβ42 (i.e., dodecamer), but the oligomer *distributions* are dramatically different from that of wt Aβ42. Both Aβ42 E22G and D7N mutants form very stable dodecamer and decamer assemblies and few smaller oligomers at low injection voltages (Scheme 2b).

Unique to the Flemish mutation is a decreased rate of protfibril and fibril formation.[16] Furthermore, in a previous study,[24] the A21G peptide formed a greater abundance of Aβ42 paranuclei (n = 5, 6), compared with wt Aβ42. This is consistent with the results presented here, in which Aβ42 A21G does not form any species larger than a hexamer (Figure 4b), in contrast to wt Aβ42 that also forms stacked dihexamers[3a,b] (Figure 3b). In this study, the Aβ42 A21G hexamer has a cross section that is ∼10% greater than those of other alloforms. Moreover, the cross section reaches the upper limit of the modeled hexamer cross section, which represents the largest possible cross section for a given arrangement. This result points to a change in the structure of Aβ42 A21G hexamers. The most straightforward interpretation is that the A21G isoform forms an open (rather than cyclic) hexamer. While other explanations are possible (e.g., larger spacing between monomers in the planar hexamer ring structure and less monomer/monomer overlap) Occam's razor points to the open hexamer as the simplest solution. This open structure is also consistent with the fact that A21G does not form a dodecamer. In all other Aβ42 alloforms dodecamers are formed and are unambiguously composed of stacked hexamer rings. An open A21G hexamer might prevent the formation of this stable dodecamer structure.

Like many FAD mutations that occur within the Aβ sequence, the Flemish mutation produces both parenchymal and vascular amyloid deposits.[10,14] The dominance of small Aβ42 A21G oligomers (n ≤ 6) with unique (open) structures and the decreased propensity to form fibrils could very well allow the peptide to penetrate vessel walls more easily, resulting in the cerebrovascular events typically experienced by patients with the Flemish mutation. In contrast, the Tottori and Arctic mutants, which quickly form large assemblies, do not result in such prominent cerebrovascular pathology.

Clearly, all three substitutions alter the oligomerization of Aβ compared with the wild-type peptide (Schemes 1 and 2). It is expected that the mutations cause differences in the monomer structures. Due to the natively disordered nature of these peptides,[30] however, it is not surprising that their monomer cross sections are very similar. If structural differences are indeed present, they appear to be reflected in the assembly process. Pathologically this is evident in the different ways FAD develops and expresses itself for the different mutants. Here we show that as assembly takes place D7N, A21G, and E22G all exhibit strikingly different oligomer distributions for both Aβ40 and Aβ42 between themselves and when compared with wild-type. These differences are shown to be consistent with other reported experimental results that deal with protofibril and fibril formation.[11−13,16,17] While there also appears to be some correlation between oligomer distributions and disease pathology, it is not yet possible to establish a definitive mechanistic connection. However, now that these assembly differences have been established, there is hope that such a connection can be made in the future.

■ METHODS

IM-MS Experiments. The FAD-related Tottori (D7N), Flemish (A21G), and Arctic (E22G) mutations of Aβ40 and Aβ42 were synthesized by FMOC (N-(9-fluorenyl)methoxycarbonyl) chemistry. The samples were purified by reverse-phase HPLC, characterized by mass spectrometry and amino acid analysis,[12] and lyophilized. The lyophilized peptide was dissolved in 10 mM ammonium acetate (pH 7.4) to a final concentration of 20 μM. All mass spectra and ion

mobility data were recorded on a home-built ion mobility mass spectrometer.[26]

For mass spectrometry experiments, ions are generated continuously by a nanoelectrospray ionization source, guided through an ion funnel, and focused into a 4.503 cm long temperature-controlled drift cell containing helium at a pressure of 4 Torr. After passing through the cell, the ions are mass-selected by a quadrupole mass filter and detected.

For ion-mobility measurements, ions are stored in the ion funnel and pulsed into the drift cell. The injection voltage can be varied from near 0 to 100 eV. At low injection voltages, the ions are rapidly thermalized by cooling collisions with the helium buffer gas in the cell. At high injection voltages, the ions are given energy that can lead to internal excitation, before reaching thermal equilibrium. This transient internal excitation can cause either annealing (isomerization) into a lower energy structure or dissociation of large noncovalent complexes into smaller subcomponents. Once in the cell, the analyte passes through under the influence of a weak electric field. The velocity of the ions in the drift cell, v_D, is determined by the force of the electric field and the frictional drag of the collisions with the helium buffer gas. The drift velocity is proportional to the electric field, $\mathbf{E}$, with the proportionality constant, K, termed the ion mobility:

$$v_D = K \cdot \mathbf{E} \tag{1}$$

The ions are mass-selected, continuing to the detector, and their arrival times are recorded. An ion's mobility is related to the ion−He collision cross-section σ, which in turn can be related to the ion's arrival time at the detector, t_A:[27]

$$\sigma = 1.3 \left(\frac{q^2 E^2 T}{\mu k_B N^2 l^2} \right)^{1/2} (t_A - t_0) \tag{2}$$

Here, q is the ion charge, k_B is the Boltzmann constant, T is the temperature, μ is the reduced mass of the ion−He collision, N is the He number density at STP, l is the drift cell length (4.503 cm), and t_0 is the time the ion spends outside of the drift cell. The quantities are either known constants or are measured for each experiment so that σ can be determined.

Peak Fitting. Experimental ATDs can be fit by calculating the flux of ions exiting the drift tube using the ion transport equation[28] given by eq 3:

$$I(t) = \frac{I_0}{4(\pi D_L t)^2} \left(v_d + \frac{z}{t} \right) \left[1 - \exp\left(-\frac{r_o^2}{4 D_T t} \right) \right]$$
$$\exp\left[-\frac{(z - v_d t)^2}{4 D_L t} \right] \tag{3}$$

where z is the ion charge and r_o is the radius of the initial ion packet, z is the cell length, and v_d is the drift velocity through the tube. The ion packet drifts through a tube of length in a uniform electric field and undergoes longitudinal and transverse diffusion (D_L and D_T). The diffusion coefficients, D_L and D_T, may be approximated by

$$D = \frac{k_B T K}{e} \tag{4}$$

where e is the ion's charge, T is the temperature, K is the experimental mobility, and k_B is the Boltzmann constant. The fitted peak represents the expected ATD for a species with a given cross section. If a peak in the experimental ATD is broader than its fit, then the peak likely represents a family of structures, rather than a single structure.

Modeling of Aβ Oligomers. The Aβ oligomers studied here are too large for analysis with current molecular dynamics methods. Instead, the cross sections of various oligomers (tetramer through dodecamer) were approximated with a simple structural model, which has been previously used to describe the oligomer states of wt Aβ.[3a] Each monomer is assumed to be spherical, with a monomer cross section equal to that measured by the IM-MS experiment. The dimer cross section of each peptide was determined by fitting the center−

center distance between the two monomer spheres to the experimental cross sections of the dimer. Using the center−center distance as a variable parameter allowed for the determination of the degree of "overlap" between two monomer structures within a dimer. Once determined, the degree of overlap was kept constant for all other model structures. Two notable exceptions are Aβ42 D7N and Aβ42 E22G, for which no experimental dimer cross sections were available (see Results section). In these cases, the overlap for wt Aβ42 was used, although the cross sections of each modeled peptide (i.e., each sphere) within the oligomers were consistent with their own respective monomer cross sections. This assumption will alter the resulting cross sections somewhat, although we do not expect it to cause a dramatic change in the data. All monomers overlap to similar extents, such that the cross sections of oligomers of similar arrangements vary only 1−3% between alloforms.

Geometries for each model were built in Molden.[29] Oligomer geometries are shown in Table 2 and were chosen to span a range of assembly sizes, with the goal of calculating extreme sizes (i.e., the largest and smallest possible structures; see Supporting Information for discussion of selected structures). Cross sections for each modeled structure were calculated using Sigma[30] and are listed in Table 2. As described previously,[3a] the cross section of each individual peptide within an oligomer shrinks as the oligomeric order (n) increases, due to increasing amounts of overlap and structural accommodation of monomer Aβ within oligomers, although this effect is not expected to be large (∼10%). Because of this, the model produces cross sections that are upper limits to the experimental cross sections. These model cross sections were then compared with experimental cross sections of features in complex ATDs in order to determine peak assignments (see Table 2 for comparison and Supporting Information for an example of a more detailed comparison).

■ ASSOCIATED CONTENT

ⓢ Supporting Information

Additional IM-MS data of Aβ peptides, including mass spectra for each mutant of Aβ40 and Aβ42, all ATDs of $z/n = -3$, and injection energy studies and additional discussion of the oligomer models. This material is available free of charge via the Internet at http://pubs.acs.org.

■ AUTHOR INFORMATION

Notes

The authors declare no competing financial interest.

■ ACKNOWLEDGMENTS

We thank Margaret Condron for synthesizing the Aβ peptides used in this work.

■ ABBREVIATIONS

FAD, Familial Alzheimer's disease; Aβ, amyloid β-protein; IM-MS, ion mobility mass spectrometry; ATD, arrival time distribution

■ REFERENCES

(1) Roychaudhuri, R., Yang, M., Hoshi, M. M., and Teplow, D. B. (2009) Amyloid β-protein assembly and Alzheimer disease. *J. Biol. Chem.* 284 (8), 4749−4753.

(2) Dahlgren, K. N., Manelli, A. M., Stine, W. B., Baker, L. K., Krafft, G. A., and LaDu, M. J. (2002) Oligomeric and fibrillar species of amyloid-β peptides differentially affect neuronal viability. *J. Biol. Chem.* 277 (35), 32046−32053.

(3) (a) Bernstein, S. L., Dupuis, N. F., Lazo, N. D., Wyttenbach, T., Condron, M. M., Bitan, G., Teplow, D. B., Shea, J. E., Ruotolo, B. T., Robinson, C. V., and Bowers, M. T. (2009) Amyloid-β protein oligomerization and the importance of tetramers and dodecamers in the aetiology of Alzheimer's disease. *Nat. Chem. 1* (4), 326−331. (b) Bernstein, S. L., Wyttenbach, T., Baumketner, A., Shea, J. E., Bitan, G., Teplow, D. B., and Bowers, M. T. (2005) Amyloid β-protein: Monomer structure and early aggregation states of Aβ42 and its Pro(19) alloform. *J. Am. Chem. Soc. 127* (7), 2075−2084. (c) Bitan, G., Kirkitadze, M. D., Lomakin, A., Vollers, S. S., Benedek, G. B., and Teplow, D. B. (2003) Amyloid β-protein (Aβ) assembly: Aβ40 and Aβ42 oligomerize through distinct pathways. *Proc. Natl. Acad. Sci. U.S.A. 100* (1), 330−335.

(4) Tanzi, R. E. (1999) A genetic dichotomy model for the inheritance of Alzheimer's disease and common age-related disorders. *J. Clin. Invest. 104* (9), 1175−1179.

(5) Levylahad, E., Wasco, W., Poorkaj, P., Romano, D. M., Oshima, J., Pettingell, W. H., Yu, C. E., Jondro, P. D., Schmidt, S. D., Wang, K., Crowley, A. C., Fu, Y. H., Guenette, S. Y., Galas, D., Nemens, E., Wijsman, E. M., Bird, T. D., Schellenberg, G. D., and Tanzi, R. E. (1995) Candidate gene for the chormosome-1 familial Alzheimer's disease locus. *Science 269* (5226), 973−977.

(6) Kang, J., Lemaire, H. G., Unterbeck, A., Salbaum, J. M., Masters, C. L., Grzeschik, K. H., Multhaup, G., Beyreuther, K., and Mullerhill, B. (1987) The precursor of Alzheimer's disease amyloid Aβ protein resembles a cell-surface receptor. *Nature 325* (6106), 733−736.

(7) Sherrington, R., Rogaev, E. I., Liang, Y., Rogaeva, E. A., Levesque, G., Ikeda, M., Chi, H., Lin, C., Li, G., Holman, K., Tsuda, T., Mar, L., Foncin, J. F., Bruni, A. C., Montesi, M. P., Sorbi, S., Rainero, I., Pinessi, L., Nee, L., Chumakov, I., Pollen, D., Brookes, A., Sanseau, P., Polinsky, R. J., Wasco, W., Dasilva, H. A. R., Haines, J. L., Pericakvance, M. A., Tanzi, R. E., Roses, A. D., Fraser, P. E., Rommens, J. M., and Stgeorgehyslop, P. H. (1995) Cloning of a gene bearing missense mutations in early-onset familial Alzheimer's-disease. *Nature 375* (6534), 754−760.

(8) (a) Borchelt, D. R., Thinakaran, G., Eckman, C. B., Lee, M. K., Davenport, F., Ratovitsky, T., Prada, C. M., Kim, G., Seekins, S., Yager, D., Slunt, H. H., Wang, R., Seeger, M., Levey, A. I., Gandy, S. E., Copeland, N. G., Jenkins, N. A., Price, D. L., and Younkin, S. G. (1996) Familial Alzheimer's disease-linked presenilin 1 variants elevate Aβ 1−42/1−40 ratio in vitro and in vivo. *Neuron 17* (5), 1005−1013. (b) Scheuner, D., Eckman, C., Jensen, M., Song, X., Citron, M., Suzuki, N., Bird, T. D., Hardy, J., Hutton, M., Kukull, W., Larson, E., LevyLahad, E., Viitanen, M., Peskind, E., Poorkaj, P., Schellenberg, G., Tanzi, R., Wasco, W., Lannfelt, L., Selkoe, D., and Younkin, S. (1996) Secreted amyloid β-protein similar to that in the senile plaques of Alzheimer's disease is increased in vivo by the presenilin 1 and 2 and APP mutations linked to familial Alzheimer's disease. *Nat. Med. 2* (8), 864−870.

(9) Wakutani, Y., Watanabe, K., Adachi, Y., Wada-Isoe, K., Urakami, K., Ninomiya, H., Saido, T. C., Hashimoto, T., Iwatsubo, T., and Nakashima, K. (2004) Novel amyloid precursor protein gene missense mutation (D678N) in probable familial Alzheimer's disease. *J. Neurol., Neurosurg. Psychiatry 75* (7), 1039−1042.

(10) Hendriks, L., Vanduijn, C. M., Cras, P., Cruts, M., Vanhul, W., Vanharskamp, F., Warren, A., McInnis, M. G., Antonarakis, S. E., Martin, J. J., Hofman, A., and Vanbroeckhoven, C. (1992) Presenile-dementia and cerebral-hemorrhage linked to a mutation at codon 692 of the β-amyloid precursor protein gene. *Nat. Genet. 1* (3), 218−221.

(11) Nilsberth, C., Westlind-Danielsson, A., Eckman, C. B., Condron, M. M., Axelman, K., Forsell, C., Stenh, C., Luthman, J., Teplow, D. B., Younkin, S. G., Naslund, J., and Lannfelt, L. (2001) The 'Arctic' APP mutation (E693G) causes Alzheimer's disease by enhanced Aβ protofibril formation. *Nat. Neurosci. 4* (9), 887−893.

(12) Hori, Y., Hashimoto, T., Wakutani, Y., Urakami, K., Nakashima, K., Condron, M. M., Tsubuki, S., Saido, T. C., Teplow, D. B., and Iwatsubo, T. (2007) The Tottori (D7N) and English (H6R) familial Alzheimer disease mutations accelerate Aβ fibril formation without increasing protofibril formation. *J. Biol. Chem. 282* (7), 4916−4923.

(13) Ono, K., Condron, M. M., and Teplow, D. B. (2010) Effects of the English (H6R) and Tottori (D7N) Familial Alzheimer Disease Mutations on Amyloid β-Protein Assembly and Toxicity. *J. Biol. Chem. 285* (30), 23184−23195.

(14) Roks, G., Van Harskamp, F., De Koning, I., Cruts, M., De Jonghe, C., Kumar-Singh, S., Tibben, A., Tanghe, H., Niermeijer, M. F., Hofman, A., Van Swieten, J. C., Van Broeckhoven, C., and Van Duijn, C. M. (2000) Presentation of amyloidosis in carriers of the codon 692 mutation in the amyloid precursor protein gene (APP692). *Brain 123*, 2130−2140.

(15) (a) Haass, C., Hung, A. Y., Selkoe, D. J., and Teplow, D. B. (1994) Mutations associated with a locus for familial Alzheimer's disease result in alternative processing of amyloid β-protein precursor. *J. Biol. Chem. 269* (26), 17741−17748. (b) Betts, V., Leissring, M. A., Dolios, G., Wang, R., Selkoe, D. J., and Walsh, D. M. (2008) Aggregation and catabolism of disease-associated intra-Aβ mutations: Reduced proteolysis of A beta A21G by neprilysin. *Neurobiol. Dis. 31* (3), 442−450.

(16) Murakami, K., Irie, K., Morimoto, A., Ohigashi, H., Shindo, M., Nagao, M., Shimizu, T., and Shirasawa, T. (2002) Synthesis, aggregation, neurotoxicity, and secondary structure of various Aβ1−42 mutants of familial Alzheimer's disease at positions 21−23. *Biochem. Biophys. Res. Commun. 294* (1), 5−10.

(17) Bitan, G., Vollers, S. S., and Teplow, D. B. (2003) Elucidation of primary structure elements controlling early amyloid β-protein oligomerization. *J. Biol. Chem. 278* (37), 34882−34889.

(18) (a) Levy, E., Carman, M. D., Fernandezmadrid, I. J., Power, M. D., Lieberburg, I., Vanduinen, S. G., Bots, G., Luyendijk, W., and Frangione, B. (1990) Mutations of the Alzheimer's-disease amyloid gene in hereditary cerbral-hemorrhage, Dutch type. *Science 248* (4959), 1124−1126. (b) De Jonghe, C., Zehr, C., Yager, D., Prada, C. M., Younkin, S., Hendriks, L., Van Broeckhoven, C., and Eckman, C. B. (1998) Flemish and Dutch mutations in amyloid β precursor protein have different effects on amyloid β secretion. *Neurobiol. Dis. 5* (4), 281−286. (c) Grabowski, T. J., Cho, H. S., Vonsattel, J. P. G., Rebeck, G. W., and Greenberg, S. M. (2001) Novel amyloid precursor protein mutation in an Iowa family with dementia and severe cerebral amyloid angiopathy. *Ann. Neurol. 49* (6), 697−705.

(19) Klyubin, I., Walsh, D. M., Cullen, W. K., Fadeeva, J. V., Anwyl, R., Selkoe, D. J., and Rowan, M. J. (2004) Soluble Arctic amyloid β protein inhibits hippocampal long-term potentiation in vivo. *Eur. J. Neurol. 19* (10), 2839−2846.

(20) Cheng, I. H., Scearce-Levie, K., Legleiter, J., Palop, J. J., Gerstein, H., Bien-Ly, N., Puolivali, J., Lesne, S., Ashe, K. H., Muchowski, P. J., and Mucke, L. (2007) Accelerating amyloid-β fibrillization reduces oligomer levels and functional deficits in Alzheimer disease mouse models. *J. Biol. Chem. 282* (33), 23818−23828.

(21) (a) Lesne, S., Koh, M. T., Kotilinek, L., Kayed, R., Glabe, C. G., Yang, A., Gallagher, M., and Ashe, K. H. (2006) A specific amyloid-β protein assembly in the brain impairs memory. *Nature 440* (7082), 352−357. (b) Shankar, G. M., Li, S., Mehta, T. H., Garcia-Munoz, A., Shepardson, N. E., Smith, I., Brett, F. M., Farrell, M. A., Rowan, M. J., Lemere, C. A., Regan, C. M., Walsh, D. M., Sabatini, B. L., and Selkoe, D. J. (2008) Amyloid-β protein dimers isolated directly from Alzheimer's brains impair synaptic plasticity and memory. *Nat. Med. 14* (8), 837−842. (c) Kirkitadze, M. D., Bitan, G., and Teplow, D. B. (2002) Paradigm shifts in Alzheimer's disease and other neuro degenerative disorders: The emerging role of oligomeric assemblies. *J. Neurosci. Res. 69* (5), 567−577.

(22) Wyttenbach, T., and Bowers, M. T. (2003) Gas-phase conformations: The ion mobility/ion chromatography method. *Mod. Mass Spectrom. 225*, 207−232.

(23) Baumketner, A., Bernstein, S. L., Wyttenbach, T., Bitan, G., Teplow, D. B., Bowers, M. T., and Shea, J. E. (2006) Amyloid β-protein monomer structure: A computational and experimental study. *Protein Sci. 15* (3), 420−428.

(24) Ono, K., Condron, M. M., and Teplow, D. B. (2009) Structure-neurotoxicity relationships of amyloid β-protein oligomers. *Proc. Natl. Acad. Sci. U.S.A. 106* (35), 14745−14750.

(25) Ahmed, M., Davis, J., Aucoin, D., Sato, T., Ahuja, S., Aimoto, S., Elliott, J. I., Van Nostrand, W. E., and Smith, S. O. (2010) Structural conversion of neurotoxic amyloid-β(1−42) oligomers to fibrils. *Nat. Struct. Mol. Biol. 17* (5), 561−567.

(26) Wyttenbach, T., Kemper, P. R., and Bowers, M. T. (2001) Design of a new electrospray ion mobility mass spectrometer. *Int. J. Mass Spectrom. 212* (1−3), 13−23.

(27) Gidden, J., Baker, E. S., Ferzoco, A., and Bowers, M. T. (2005) Structural motifs of DNA complexes in the gas phase. *Int. J. Mass Spectrom. 240* (3), 183−193.

(28) Mason, E. A., and McDaniel, E. W. (1988) *Transport Properties of Ions in Gases*, pp xvi, 560, Wiley, New York.

(29) Schaftenaar, G., and Noordik, J. H. (2000) Molden: A pre- and post-processing program for molecular and electronic structures. *J. Comput.-Aided Mol. Des. 14* (2), 123−134.

(30) (a) Vonhelden, G., Hsu, M. T., Gotts, N., and Bowers, M. T. (1993) Carbon cluster cations with up to 84 atoms-structures, formation mechanism, and reactivity. *J. Phys. Chem. 97* (31), 8182−8192. (b) Wyttenbach, T., von Helden, G., Batka, J. J., Carlat, D., and Bowers, M. T. (1997) Effect of the long-range potential on ion mobility measurements. *J. Am. Soc. Mass Spectom. 8* (3), 275−282.